frontiers | Frontiers in Astronomy and Space Sciences

TYPE Original Research
PUBLISHED 20 December 2024
DOI 10.3389/fspas.2024.1507824

Check for updates

OPEN ACCESS

EDITED BY
Joseph E Borovsky,
Space Science Institute (SSI), United States

REVIEWED BY
Yun Gong,
Wuhan University, China
Yining Shi,
University of Michigan, United States

*CORRESPONDENCE
Zan-Yang Xing,
xingzanyang@sdu.edu.cn

RECEIVED 08 October 2024
ACCEPTED 03 December 2024
PUBLISHED 20 December 2024

CITATION
Lu S, Xing Z-Y, Zhang Q-H, Zhang Y, Oksavik K, Lyons LR, Lockwood M, Ma Y-Z, Wang X-Y, Balan N, Yang H-G, Wang Y, Deng Z-X, Xu T and Sun S-J (2024) Observations of three-dimensional ionospheric plasma properties in a space hurricane.
Front. Astron. Space Sci. 11:1507824.
doi: 10.3389/fspas.2024.1507824

COPYRIGHT
© 2024 Lu, Xing, Zhang, Zhang, Oksavik, Lyons, Lockwood, Ma, Wang, Balan, Yang, Wang, Deng, Xu and Sun. This is an open-access article distributed under the terms of the Creative Commons Attribution License (CC BY). The use, distribution or reproduction in other forums is permitted, provided the original author(s) and the copyright owner(s) are credited and that the original publication in this journal is cited, in accordance with accepted academic practice. No use, distribution or reproduction is permitted which does not comply with these terms.

Observations of three-dimensional ionospheric plasma properties in a space hurricane

Sheng Lu[1], Zan-Yang Xing[1]*, Qing-He Zhang[1,2], Yongliang Zhang[3], Kjellmar Oksavik[4,5], L. R. Lyons[6], Michael Lockwood[7], Yu-Zhang Ma[1], Xiang-Yu Wang[1], N. Balan[1], Hui-Gen Yang[1,8], Yong Wang[1], Zhong-Xin Deng[9], Tong Xu[9] and Shu-Ji Sun[9]

[1]Shandong Provincial Key Laboratory of Optical Astronomy and Solar-Terrestrial Environment, Institute of Space Sciences, Shandong University, Weihai, China, [2]State Key Laboratory of Space Weather, Center for Space Science and Applied Research, Chinese Academy of Sciences, Beijing, China, [3]Applied Physics Laboratory, The Johns Hopkins University, Laurel, MD, United States, [4]Department of Physics and Technology, University of Bergen, Bergen, Norway, [5]Arctic Geophysics, University Centre in Svalbard, Longyearbyen, Norway, [6]Department of Atmospheric and Oceanic Sciences, University of California, Los Angeles, Los Angeles, CA, United States, [7]Department of Meteorology, University of Reading, Reading, United Kingdom, [8]Polar Research Institute of China, Shanghai, China, [9]China Research Institute of Radiowave Propagation, Qingdao, China

The space hurricane is a newly discovered large-scale three-dimensional magnetic vortex structure that spans the polar ionosphere and magnetosphere. It has been suggested to open a fast energy transport channel for the solar wind to invade Earth's magnetosphere under northward interplanetary magnetic field (IMF) conditions. It is, therefore, an important phenomenon to understand the solar wind–magnetosphere–ionosphere coupling process under northward IMF conditions. In this study, we report the three-dimensional ionospheric plasma properties of a space hurricane event in the Northern Hemisphere observed by multiple instruments. Based on the convection velocity observations from ground-based radars and polar satellites, we confirm that the major modulation to the polar cap convection called a space hurricane rotates clockwise at the altitude of the ionosphere. Ground-based incoherent scatter radar and polar satellite observations reveal four features associated with the space hurricane: 1) strong plasma flow shears and being embedded in a clockwise lobe convection cell; 2) a major addition to the total energy deposition in the ionosphere–thermosphere system by Joule heating; 3) downward ionospheric electron transport; and 4) multiple ion-temperature enhancements in the sunward velocity region, likely from the spiral arms of the space hurricane. These results present, first, the impact of space hurricane on the low-altitude ionosphere and provide additional insights on the magnetospheric impact on structuring in the polar ionosphere.

KEYWORDS

space hurricane, polar ionosphere, polar cap aurora, particle precipitation, high-latitude lobe reconnection

1 Introduction

Aurora is the result of the interaction between precipitating particles energized by the solar wind with various atoms in the upper atmosphere. Most auroras occur in two continuous "aurora ovals" around each geomagnetic pole. A few auroras can also be seen inside the "polar cap" as spots or arcs that are referred to as "polar cap arcs" or "polar cap spots" (Hosokawa et al., 2020; Kullen, 2012; Zhu et al., 1997). The polar cap auroras discovered by spacecraft include transpolar arcs (e.g., Berkey et al., 1976; Fear and Milan, 2012; A. Kullen et al., 2015; Xing et al., 2018; Q.-H. Zhang et al., 2020; Y. Zhang et al., 2016), 15MLT-polar cap arc (Han et al., 2020), space hurricane (Q.-H. Zhang et al., 2021), and high-latitude dayside aurora, (e.g., Cai et al., 2021; H. U. Frey et al., 2003; Korth et al., 2004). Among these, the space hurricane is not only a bright cyclone-shaped aurora near the magnetic pole but also a large-scale magnetic vortex structure that spans the polar ionosphere and magnetosphere, which opens a strong energy transport channel from the solar wind to Earth's magnetosphere (Q.-H. Zhang et al., 2021). In the Northern Hemisphere, the space hurricane occurs mainly in summer with a maximum occurrence rate in the afternoon sector under a northward interplanetary magnetic field (IMF) dominated by a positive By component (Lu et al., 2022). The higher occurrence in the Southern hemisphere is consistent with magnetic reconnection on the sunward edge of the tail lobe during the northward IMF, as inferred from satellite data (Crooker and Rich, 1993; Rich and Hairston, 1994), Super Dual Auroral Radar Network (SuperDARN) studies (Koustov et al., 2017), field-aligned current observations (Reistad et al., 2019; 2021), and a survey of 23 years of polar cap index data (Lockwood, 2023). It can cause unusual energy injection under the northward IMF, and so, the space hurricane is very important for understanding the magnetosphere–ionosphere–thermosphere coupling under the northward IMF. In addition, some studies have shown that the injection of energy into the polar ionosphere can cause strong scintillation and communication anomalies (e.g., Oksavik et al., 2015; Prikryl et al., 2010; 2014; Wang et al., 2021; Q.-H. Zhang et al., 2017), suggesting that the space hurricane may also impose space weather challenges.

Some studies of polar cap auroras have revealed their formation mechanism and their association with ionospheric flows (particularly flow shears and vortices) by observing their structure and plasma characteristics. Frey et al. (2003) found an aurora spot in the dayside polar cap and named it "HiLDA." The coincident plasma observation revealed that the strong precipitation of field-aligned accelerated electrons causes the aurora, which is related to high-latitude magnetopause reconnection. Cai et al., (2021), using the Special Sensor Ultraviolet Spectrographic Imager (SSUSI) onboard the Defense Meteorological Satellite Program (DMSP) satellite, analyzed some arc-like aurora (Han et al., 2020) cases in the polar cap. They found that the arc-like aurora forms in the polar cap when the clockwise convection cell is not well formed due to the weaker lobe reconnection under the positive IMF By and Bz ~ 0. Regarding the space hurricane, also located inside the polar cap, some features that have been reported from DMSP satellite observations at an 860-km altitude include a circular horizontal plasma flow, a nearly zero-flow center, and a coincident cyclone-shaped aurora caused by strong electron precipitation associated with upward field-aligned currents (Q.-H. Zhang et al., 2021). However, many features of the space hurricane at ionospheric altitudes remain unknown.

In this paper, we examine a space hurricane event observed by the Resolute Bay Incoherent Scatter Radar North (RISR-N), SuperDARN radars, and DMSP satellites. We obtain the 3D ionospheric plasma properties of the space hurricane for the first time and reveal further novel and critical results about this phenomenon. This work adds to our knowledge and understanding about the magnetospheric impact on the structure of the polar cap ionosphere under a northward IMF.

2 Data and methodology

In this study, the space hurricane event was observed by multiple instruments at the same time. The Time History of Events and Macroscale Interactions during Substorms (THEMIS) B satellite, located in the lunar orbit and within the solar wind, was used to determine the IMF conditions during the space hurricane event. The DMSP satellite crossed the space hurricane twice during the study period, providing data from an 860-km altitude on the auroral emissions, plasma characteristics, and location of the space hurricane. The RISR-N radar conducted multiple scans of the space hurricane, offering plasma parameters within the 100–400-km altitude range. Meanwhile, the SuperDARN radar was used to provide plasma convection data at approximately 350-km altitude (F-region). The detailed descriptions of these instruments and data are discussed as follows.

2.1 THEMIS IMF data

In this study, the THEMIS B satellite was used to obtain near-Earth interplanetary parameters (Angelopoulos, 2008). Consider the distance of the THEMIS B satellite from the dayside ionosphere and the average speed of the solar wind. A 15-min delay was applied to the IMF data recorded by THEMIS B (Liou et al., 1998; Lockwood et al., 1989; Lockwood, 2022).

2.2 DMSP data

The DMSP spacecraft operates in a Sun-synchronous orbit at an altitude of 860 km, with an orbital period of approximately 101 min. During the space hurricane event analyzed in this study, three DMSP satellites (F16, F17, and F18) were active. These satellites are equipped with four types of instruments that provide auroral and local plasma observations: the SSUSI, Special Sensor for Ions, Electrons, and Scintillation (SSIES), Fluxgate Magnetometer (SSM), and Precipitating Electron and Ion Spectrometer (SSJ/4). The SSUSI captures horizon-to-horizon auroral images across five far-ultraviolet wavelengths, and in this study, data from the Lyman–Birge–Hopfield short (LBHS, 140–150 nm) band were used. The SSJ/4 instrument monitors precipitating particles within an energy range of 32 eV–30 keV, with a temporal resolution of 1 s. The SSIES includes a drift meter, retarding potential analyzer, and Langmuir probe to measure thermal ion and electron properties—such as density, temperature, and velocity—also at a

1-s resolution. Lastly, the SSM measures local magnetic fields, allowing for the estimation of field-aligned currents (FACs) based on magnetic field gradients along the spacecraft's trajectory (Hardy et al., 1984; Rich and Hairston, 1994).

2.3 RISR-N data

The RISR-N is a northward-facing, electronically steerable phased-array antenna located in Resolute Bay, Canada (74.7°N, 265.1°E). It provides direct three-dimensional measurements of the deep polar cap ionosphere, including parameters such as electron temperature, electron density, ion temperature, and line-of-sight velocity, within an altitude range of 100–400 km (Bahcivan et al., 2010). In this study, the beam pointing direction was determined on a pulse-to-pulse basis, enabling simultaneous multi-beam measurements when data were integrated over intervals of seconds or longer. For the data analyzed in this paper, the radar utilized 11 beams with varying azimuth and elevation angles, with measurements processed at a 1-min resolution. Among the 11 beams, beam 56954 (an azimuth angle of 26° and elevation angle of 35°) provided the most comprehensive coverage of the space hurricane. Additionally, four other beams (beams 65486, 57656, 60617, and 57782) were used to characterize the features of different regions surrounding the space hurricane simultaneously.

2.4 SuperDARN data

SuperDARN is a network of over 30 high-frequency (HF) radars that monitor plasma flow variations in the mid- and high-latitude ionosphere in both hemispheres. These radars operate at frequencies between 8 and 20 MHz, transmitting HF signals that are backscattered by magnetic field-aligned density irregularities in the F-region ionosphere and received back at the radar sites (Greenwald et al., 1985). The movement of these irregularities corresponds to the background ionospheric plasma flow (Villain et al., 1985), enabling the estimation of the flow's line-of-sight component via the Doppler shift of the returned signal. The SuperDARN radars transmit in narrow beams approximately 3.25° wide and typically sample 70–150 range gates, each 45 km in size, along the beams. They scan 16–24 beam directions within a 1 or 2-min cycle, covering an azimuthal area of roughly 52°–78° (Nishitani et al., 2019). This study used estimates of ionospheric plasma flow velocity derived from line-of-sight Doppler velocity measurements of plasma flow from SuperDARN (Ruohoniemi and Baker, 1998). The fitted 2-min convection data were used to describe the convection conditions near the space hurricane.

2.5 Calculation of Joule heating

Joule heating is a critical process in space weather studies, representing the dissipation of energy due to the interaction of ionospheric currents with the neutral atmosphere. In the ionosphere, electric fields are typically generated by interactions between the solar wind and Earth's magnetosphere, driving plasma convection and currents in high-latitude regions. The collisions between ions and neutral particles dissipate this current energy as Joule heating, resulting in a temperature increase in the surrounding plasma and neutral atmosphere. In this study, we utilize data provided by RISR-N, combined with modeling approaches, to calculate Joule heating within the radar's coverage area. The specific calculation methods are outlined as follows.

A statistic work (Lamarche et al., 2021) had revealed that the neutral wind (U) near RISR-N mainly points toward the magnetic pole, and the speed is very low (<100 m/s) compared with the ~1,000 m/s negative Vo (pointing to the radar) and the <500 m/s positive Vo (away from the radar) in Figure 4D. Therefore, ignoring the electric field caused by neutral wind, the Joule heating rate (q_j) can be expressed as (Fujii et al., 1999; Kurihara et al., 2009) (Equation 1)

$$q_j = \sigma_p (E_{V\times B} + U\times B)^2 \approx \sigma_p {E_{V\times B}}^2 = \sigma_p (V\times B)^2, \tag{1}$$

where V is the plasma velocity vectors and B is the geomagnetic field derived from the International Geomagnetic Reference Field (IGRF) model. The direction of B is mainly perpendicular to the ground in the polar cap, so the vertical velocity can be ignored when calculating $V\times B$, and V can be approximately replaced by the $V_{//}$ calculated from Vo observed by RISR-N. Although some studies used the local 3D ion drift velocities estimated from Vo of multiple beams to calculate the Joule heating rate (Heinselman and Nicolls, 2008; Kurihara, J., et al., 2009), these methods are not appropriate for obtaining 3D ion drift velocities near a space hurricane. These methods require that the ion drift velocities within a large region will not undergo significant changes, and Vo measured by different beams should be the components for the same velocity vector. However, this assumption is not valid near a space hurricane that has strong flow shears and different velocities near different gates. Therefore, we cannot obtain the 3D ion-drift velocities near a space hurricane from RISR-N and can approximate it with $V_{//}$.

σ_p is the Pedersen conductivity, which can be expressed as (Brekke and Hall, 1988) (Equation 2)

$$\sigma_p = \frac{N_e e}{B}\left(\frac{\Omega_e \nu_{en}}{{\Omega_e}^2 + {\nu_{en}}^2} + \frac{\Omega_i \nu_{in}}{{\Omega_i}^2 + {\nu_{in}}^2}\right), \tag{2}$$

where Ne is the electron density; e is the electron charge; $\Omega_e = eB/m_e$ and $\Omega_i = eB/m_i$ are the electron and ion gyrofrequencies, respectively; and ν_{en} and ν_{in} are the electron-neutral and ion-neutral collision frequencies, respectively. Among them, Ne is obtained from the observation of RISR-N and Ω_e is a constant. Ω_i is mainly composed of three main ions (O^+, $O_2{}^+$, and NO^+) in the ionosphere. ν_{en} and ν_{in} is considered to be mainly contributed by the collisions between electrons and these three ions (O^+, $O_2{}^+$, and NO^+) with the three main neutral components (O, O_2, and N_2). According to the theoretical formula in the Thermosphere–Ionosphere Electrodynamics General Circulation Model (TIE-GCM), calculating these parameters requires the electron temperature (Te), ion temperature (Ti), neutral component temperature (Tn), and densities of the ion components and neutral components. In this paper, *Ti* and *Te* are derived from the RISR-N observation, the densities of ion components are derived from the International Reference Ionosphere (IRI) model, and the densities of neutral components are derived from the MSIS-E-00 model.

3 Observations

3.1 Space hurricane event on 7 June 2013 in the Northern Hemisphere

Figure 1 shows a space hurricane event observed by the DMSP/SSUSI in the Northern Hemisphere and the associated IMF conditions provided by the THEMIS B satellite on 7 June 2013. The times given in Figures 1A–F are the center times of the DMSP transpolar orbit, which can also be roughly considered the time when the DMSP/SSUSI observed the space hurricane (Lu et al., 2022). Among them, Figures 1B–E show the aurora structures along the space hurricane. The yellow star is the position of RISR-N, and the mauve line represents the pointing direction of beam 56954. In Figures 1A,E, the gray line with black dots shows the associated DMSP trajectory. In Figure 1F, beams 65486, 60617, 57782, and 57656 are denoted by cyan, blue, gray, and red lines, respectively.

Figure 1G shows a stable northward IMF condition with a strong positive By component and a negative Bx component from 16:30 to 20:00 UT. This long-duration IMF situation is suitable for lobe reconnection to develop, in particular for the summer (northern) hemisphere studied here (Frey et al., 2019). Figure 1B shows the space hurricane as a bright auroral spot on the morning side in the LBHS band. Subsequently, the IMF By and Bz abruptly changed at 18:35 UT from being approximately equal (clock angle ~45°) to an orientation with By > Bz (clock angle ~70°) and stabilized for the next hour. During this period, the DMSP/SSUSI images revealed that the space hurricane had moved toward the dusk side at 19:03 UT and 19:27 UT (Figures 1C,D). After another IMF change at 19:35 UT, the space hurricane moved closer to noon (Figure 1D). In short, observations from DMSP/SSUSI show that the space hurricane moved toward the dusk side with an increase in the IMF clock angle. By the end of the period, after the IMF By component turned negative, the DMSP/SSUSI image (Figure 1F) showed a transpolar arc rather than the bright spot of a space hurricane.

Figure 2 shows the *in situ* plasma observation along the trajectories of the two DMSP satellites shown in Figures 1A, E, respectively. Both trajectories showed the typical particle features of the space hurricane, including strong circular horizontal plasma flow with shears and zero-flow center (Figure 2D), strong electron precipitation (Figure 2E) associated with intense upward magnetic field-aligned currents (Figure 2C), and clear electron inverted-V acceleration (Figure 2E). The characteristics shown in this figure are the same as those of the space hurricane reported by Q. H. Zhang et al. (2021).

Compared to the auroral morphology of the space hurricane event reported by Q. H. Zhang et al. (2021), the space hurricane in this paper exhibited neither a cyclonic-like structure nor obvious spiral arms. However, as observed from the location of the aurora and IMF condition and the plasma observations by the DMSP satellites (Figures 1A,E) passing through these structures, those aurora structures have the same characteristics as the typical space hurricane reported by Q. H. Zhang et al. (2021), which shows that they are undoubtedly space hurricanes. In addition, our previous work (Lu et al., 2022) identified 329 space hurricane events in the Northern Hemisphere from the long-term optical observation onboard DMSP F16 from 2005 to 2016. Among those events, only a few had the clear cyclone-like aurora. Therefore, it can be said that the cyclonic auroral structure with spiral arms is not necessary for defining a space hurricane event as they are vulnerable to IMF changes and limited by DMSP/SSUSI spatial resolution.

3.2 Ionospheric convection properties around the space hurricane

Figure 3 shows the coordinated observations of the DMSP satellite and ground-based radars at 19:51 UT. The measured convection velocity is overlaid on the auroral observation taken from the DMSP F16/SSUSI. The red vectors represent the cross-track horizontal ion flows measured by the DMSP F16 satellite at an altitude of 860 km. The green vectors represent the fitted 2-min convection velocity measured by SuperDARN, which correspond to an altitude of approximately 350 km, typical of the F-region in the ionosphere (Ruohoniemi, J. M., & Baker, K. B., 1998). The mauve vectors represent the horizontal plasma velocity ($V_{//}$) calculated from the line-of-sight velocity (Vo) measured by 11 beams of RISR-N at an altitude of 350 km. As the horizontal velocity near a space hurricane is much greater than the vertical velocity (as shown in Figure 5), it can be assumed that Vo measured by each beam of RISR-N (elevation angle: θ) is only contributed by the local horizontal plasma velocity (Equation 3):

$$V_{//} = V_O / cos(\theta). \tag{3}$$

The mauve vectors on the dusk side of the space hurricane are mainly toward the radar, and the mauve vectors on its morning side are away from radar. This result is consistent with the cross-track horizontal ion flows from the DMSP satellite (red vectors), which measured a sunward Vy on its dusk side and anti-sunward Vy on its dawn side. These two observations indicate that the space hurricane has a clockwise flow not only at an altitude of 860 km (DMSP) but also at altitudes of 350–400 km (RISR-N). In addition, the SuperDARN convection velocity (green vectors) further supports the observation that the space hurricane is surrounded by circular convection and embedded within the clockwise lobe convection cell.

However, it is important to note the potential sources of error in these observations. The SuperDARN convection velocities are derived from line-of-sight Doppler shifts, which require assumptions about the uniformity of plasma flows and may introduce uncertainties in the regions of complex flow patterns, such as the space hurricane. Similarly, the DMSP satellite measures ion drift in the cross-track direction, and its interpretation relies on local magnetic field models, which may not fully account for small-scale field distortions. Furthermore, differences in the spatial and temporal resolution between the instruments can introduce discrepancies when comparing measurements across multiple altitudes. Despite these potential limitations, there will not be fundamental differences in the measured velocity directions. The overall agreement between the datasets strengthens the validity of the observed clockwise circulation structure.

3.3 Plasma properties of the space hurricane from the RISR-N radar beam

The RISR-N experimental mode consists of 11 beams transmitting tri-frequency long pulses (LPs), yielding 10-km range resolution,

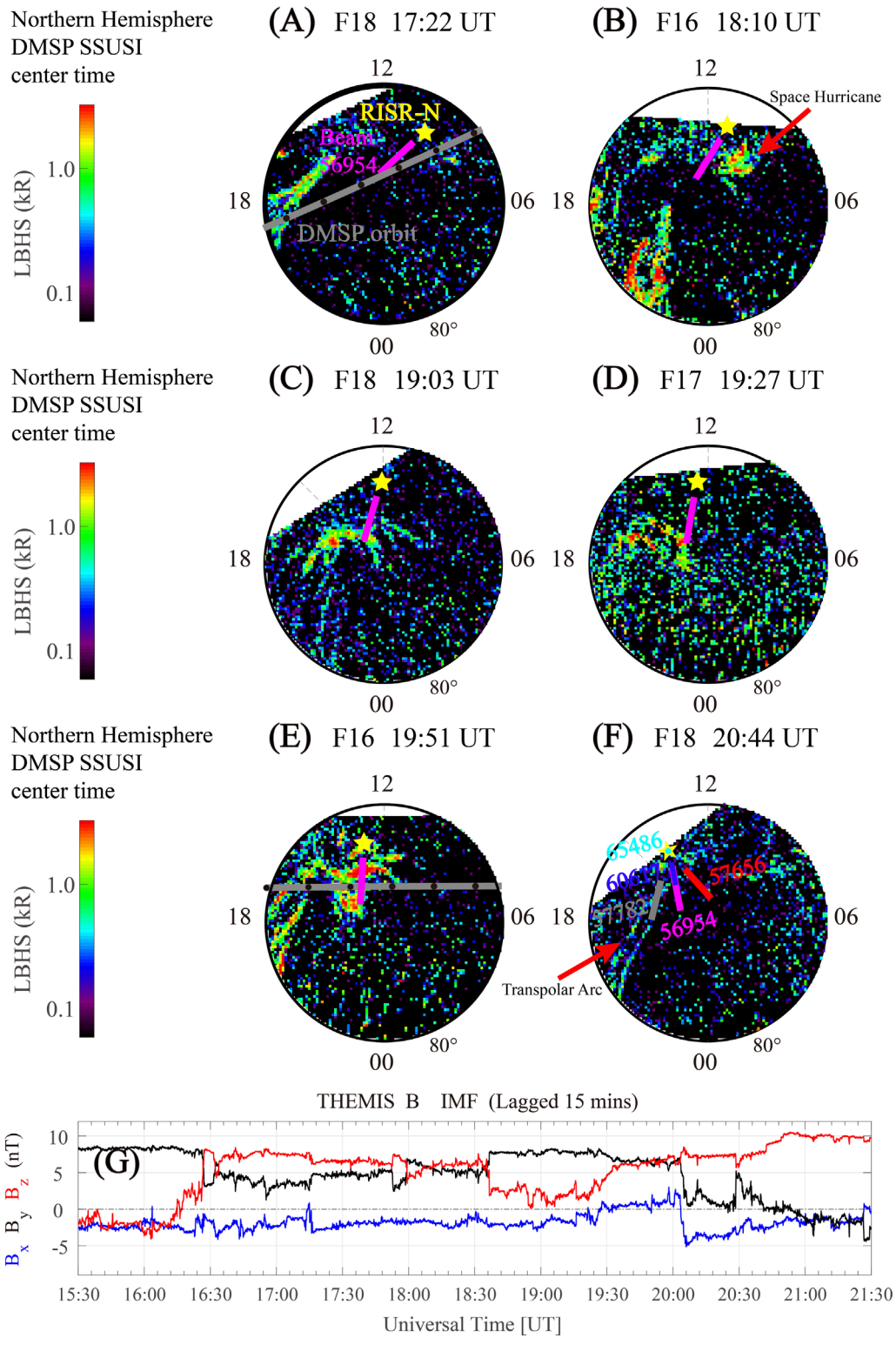

FIGURE 1
(A–F) Space hurricane event observed by the DMSP/SSUSI in the Northern Hemisphere on 7 June 2013. The yellow star denotes the position of RISR-N, and the mauve line represents the pointing direction of beam 56954. In **(A, E)**, the gray line with black dots shows the associated DMSP trajectory. In **(F)**, beams 65486, 60617, 57782 and 57656 are shown as cyan, blue, gray, and red lines, respectively. **(G)** IMF components in geocentric solar magnetosphere (GSM) coordinates provided by the THEMIS B satellite (lagged 15 min).

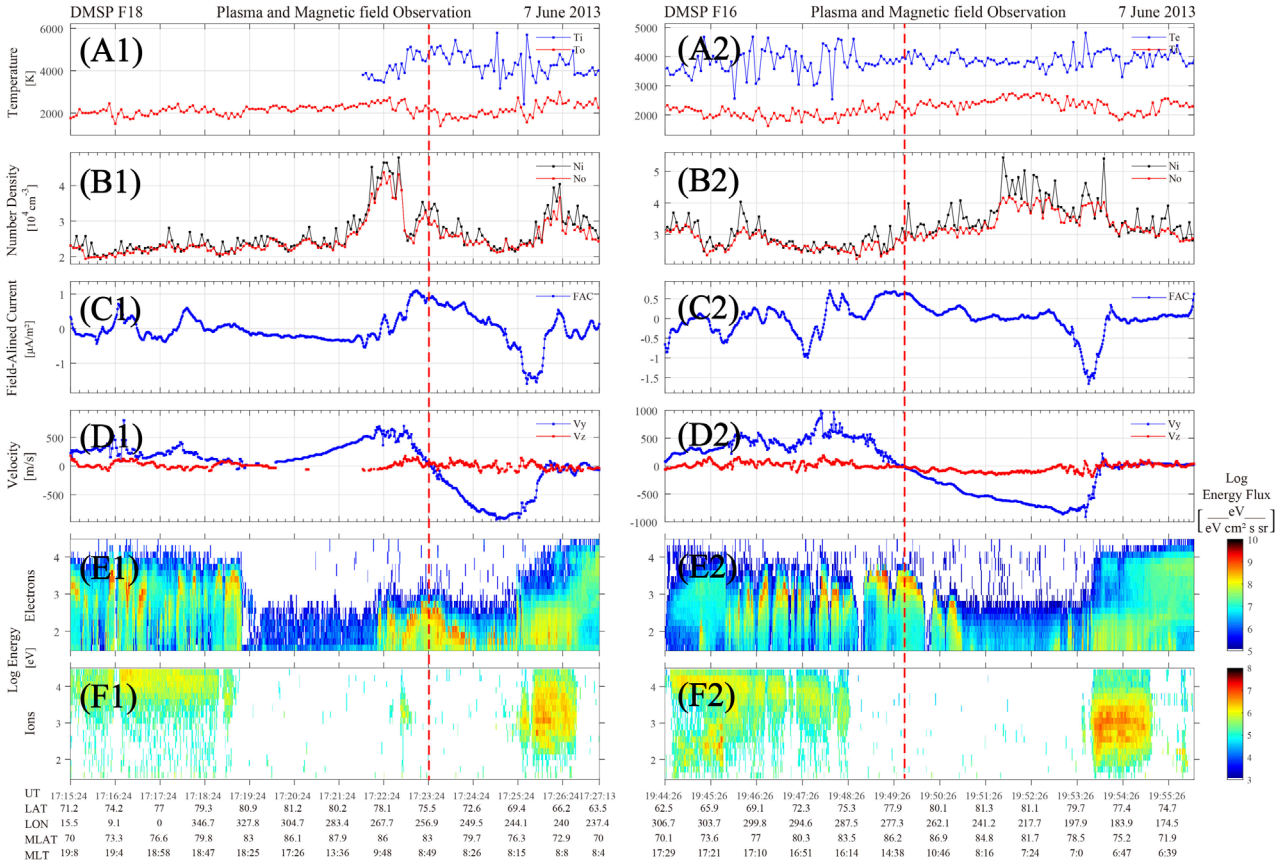

FIGURE 2
In situ plasma and current conditions for the orbit of DMSP satellites shown in Figures 1A,E, respectively. **(A)** Electron and ion temperature; **(B)** electron and ion number density; **(C)** calculated field-aligned current; **(D)** cross-track horizontal and vertical ion flow; **(E)** precipitating electron energy flux; and **(F)** precipitating ion energy flux. Data given in **(A, B, D)** are measured by the SSIES; data in panel **(C)** are calculated from the magnetic field measurement of the special sensor microwave (SSM); and data in panels €-**(F)** are measured by the Special Sensor for Precipitating Particles (SSJ4) instrument. The red dotted line marks the time when the satellite passed the center of the space hurricane. The characteristics shown in this figure are the same as those of the space hurricane reported by Zhang et al. (2021).

which was designed for F-region convection measurements. As shown in Supplementary Movie S1, RISR-N has a good coverage of the space hurricane during its evolution. To investigate its ionospheric plasma properties, we select one beam of RISR-N and show its time-series diagram from 15:30 UT to 21:30 UT in Figures 4A–D. Panels from top to bottom are electron density (Ne), electron temperature (Te), ion temperature (Ti), and line-of-sight velocity (Vo). In addition, we estimated the Joule heating rate of this beam (Figure 4E) based on the observation and models (details given in Section 2.5). The altitude/mapped magnetic latitude are shown to the left/right of each panel. The azimuth angle and elevation angle for beam 56954 are shown in the title. The directions of this beam (beam 56954) at six SSUSI image times (the center times of each transpolar orbit) are shown in Figure 1. Those six times are marked as six mauve dashed lines in Figure 4. The black dashed line in Figures 4C–E marks the enhancement of Ti, Vo, and qj, respectively.

In Figure 4, a velocity (d) reversal occurs at approximately 17:00 UT with Ti (c) enhancement in 250–400-km altitudes, which is accompanied by an Ne (a) decrease in the F-region and increase in the lower altitude (150–210 km). Based on the DMSP observation (Figure 2) and the relative position of beam 56954 at 17:22 UT (Figure 1A), we suggest that the plasma features at approximately 17:00 UT may correspond to the early stage of the space hurricane. At that time, the high-latitude lobe magnetic reconnection has just occurred and forms the upward FAC, which accelerates electron precipitation along open magnetic field lines to the ionosphere. The strong electron acceleration lowers the peak electron density of the ionosphere to below 200 km and may lead to ion heating (200–400 km) at this time. Perhaps due to the particle precipitation having just begun with relatively low precipitation energy flux (Figure 2), the auroras seen from the SSUSI are not so obvious at this time.

During 17:00~19:00 UT, the plasma properties shown in Figures 4A–D include the following: 1) Ne has a small peak below 200 km; 2) Vo is always toward the radar; 3) the Ti enhancement at a lower altitude (160–180 km) is higher than that in the F-region; and 4) the Ti enhancement corresponds one by one to Vo toward the radar (sunward flow), shown as black dashed lines in Figures 4C–E. The small Ne peak below 200 km (~20% higher than the Ne before 17 UT) may be caused by the weaker particle precipitation near its spiral arms compared to the center. The negative Vo is because the beam had been on the dusk side of the

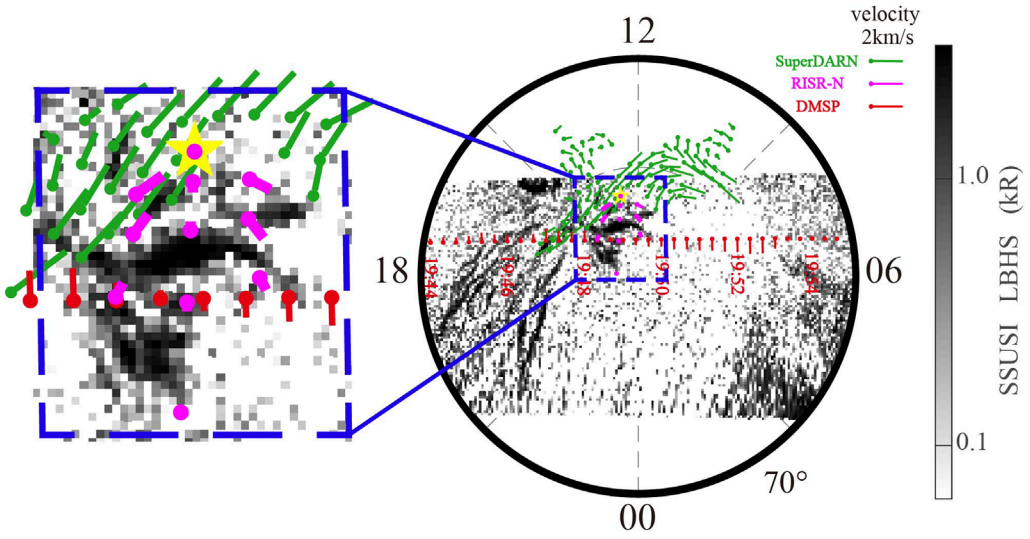

FIGURE 3
Example of aurora and convection velocity observations during the space hurricane event at approximately 19:51 UT on 7 June 2013. The red vectors represent the cross-track horizontal ion flows (Vy) measured by the DMSP F16 satellite. The mauve vectors represent the horizontal plasma velocity calculated from the line-of-sight velocity (Vo) measured by 11 beams of RISR-N at an altitude of 350 km. The green vectors represent the convection velocities measured by SuperDARN. The grayscale background is the same DMSP/SSUSI image as Figure 1E.

space hurricane during this period. Figures 1A–C show that during this period, the space hurricane moved from dawn to dusk through beam 56954. Consequently, beam 56954 should have swept through the spiral arms of the space hurricane. Thus, the fluctuations in Vo are plausibly associated with the passage of spiral arms (not discernable in the SSUSI images) through the radar field of view.

Based on the estimated Joule heating rate given in Figure 4E, it can be seen that the strong Ti enhancement at low altitudes is caused by Joule heating. Although the peak altitude of Joule heating (~150 km) is slightly lower than the peak altitude of Ti enhancement (~175 km), we suggest that this may be due to the underestimation of conductivity in the calculation process, as discussed in *Discussion*. In addition, strong Joule heating only occurs during the negative Vo periods, which may be because the negative velocity is greater than the positive velocity, and the Joule heating rate is very sensitive to the magnitude of ion drift velocity as it is proportional to the square of velocity.

After 19:00 UT, the space hurricane was no longer intersected by the beam (Figures 1C–E). Therefore, the four plasma parameters measured by RISR-N did not show any anomalies during this period. Until 19:51 UT, the space hurricane was just below the scanning range of beam 56954 (Figure 1E). The properties from 20:00 to 20:30 UT were also similar to those in the previous period (17:00~19:00 UT). The shorter duration of the Ti enhancement during this period was because the space hurricane disappeared when the suitable IMF conditions changed around 20:30 UT.

As mentioned before, RISR-N has 11 beams in this observation experiment. These beams have seven different azimuth angles, among which the beams pointing toward the North Pole have five different elevation angles. Figure 4 only shows the temporal observation results of beam 56954, which points toward the North Pole with a 35° elevation angle. To examine the characteristics of different regions in the evolution process of the space hurricane, the time-series diagram of the other four typical beams are shown in Figure 5. The directions of those beams are shown in Figure 1F.

Panels (a1)–(d1) show the observation of the vertical beam (beam 65486). It can be seen that the vertical velocity near the RISR-N did not exceed 100 m/s during the duration of the space hurricane. The maximum vertical velocity (~75 m/s) occurs near 20:00 UT when the auroral structure of a space hurricane covers RISR-N (Figure 1E), indicating that the space hurricane can cause ion upflow. In addition, compared to the ~1,000 m/s Vo measured by beam 56954 with an elevation angle of 35° (Figure 4D), the vertical velocity is small, which indicates that Vo is mainly contributed by the local horizontal plasma velocity. Panels (a2)–(d2) show the result of beam 60617, which has the same azimuth angle and a larger elevation angle than beam 56954. The same azimuth angle means it observed the same MLT of the space hurricane, while a larger elevation angle means its observations were obtained at a higher altitude but slightly farther from the space hurricane. Therefore, the ion temperature enhancement is only observed at the higher altitude, which is much closer to the space hurricane. Panels (a3)–(d3) and (a4)–(d4) show the results for two beams with the same elevation angle/altitude as beam 56954 but different azimuth angles/MLT values, which means that they observed different locations of the space hurricane at the same altitude and time. During the duration of the space hurricane (Supplementary Movie S1), the direction of beam 57782 deviates toward the dusk side, which coincides with the direction of the clockwise convection cell around the space hurricane. Therefore, a large Vo can be observed. On the other hand, the direction of beam 57656 deviates toward the dawn side. It is much closer to the space hurricane (convection cell center) than beams 57782 and 56,954 when the space hurricane is on the dawn side of the radar (before Figure 1C). Therefore, we initially observed a small Vo. However, when the space hurricane moves to the dusk side (after Figure 1C), the Vo of beam 57656 is further from the space

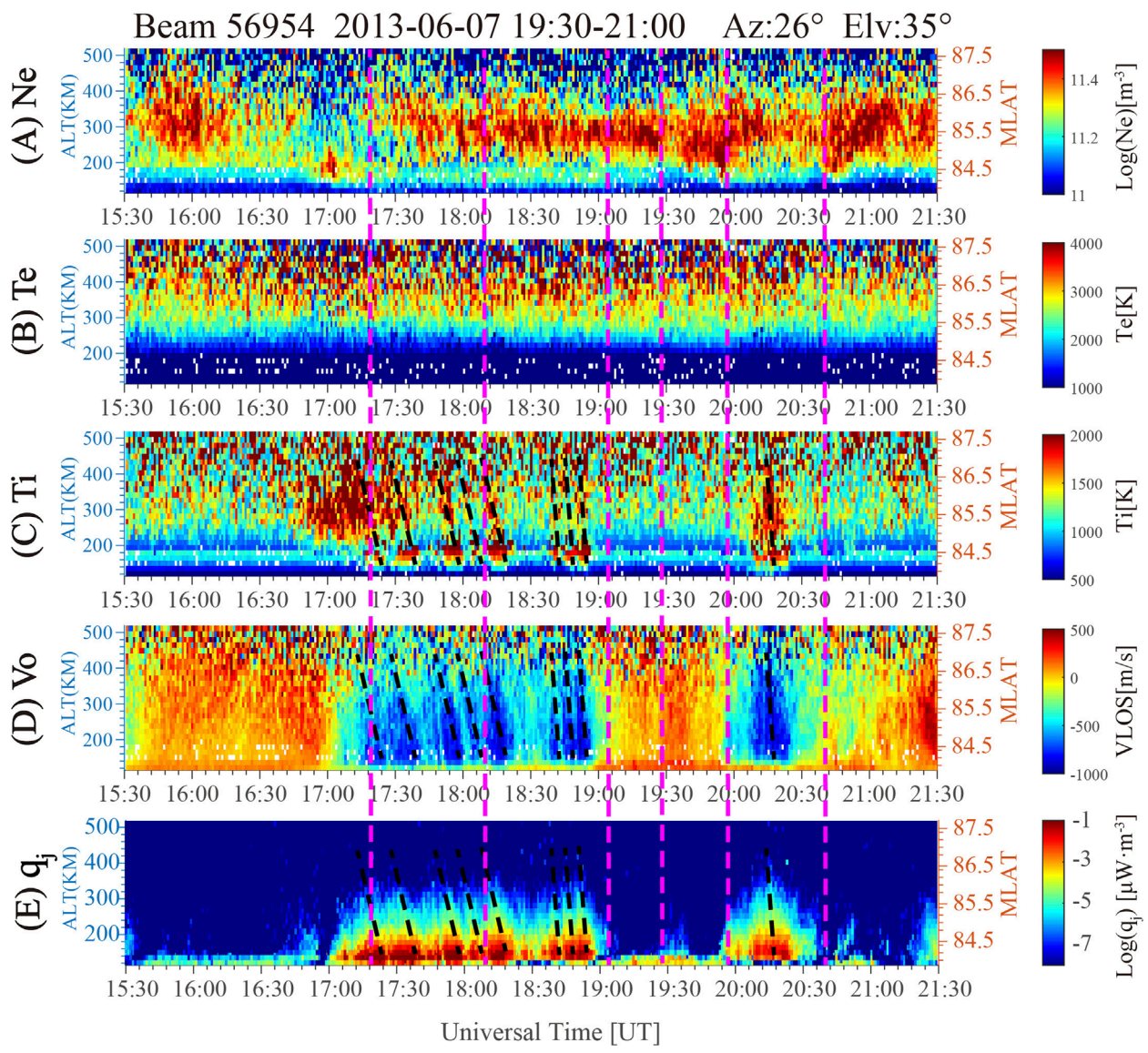

FIGURE 4
Observed plasma parameters and the calculated Joule heating rate from RISR-N beam 56954 during the space hurricane. Panels from top to bottom are electron density (Ne), electron temperature (Te), ion temperature (Ti), line-of-sight velocity (Vo), and calculated Joule heating rate (qj). The altitude/mapped magnetic latitude are shown to the left/right of each panel. The azimuth angle and elevation angle for beam 56954 are shown in the title. The six mauve dashed lines mark the six SSUSI image times shown in Figure 1. The black dashed line in **(C–E)** marks the enhancement of Ti, Vo, and qj, respectively.

hurricane and the magnitude of Vo is much higher than that of other beams. Except for Vo, other plasma properties like Ne (a) and Ti (c) from different beams are very similar to each other: Ne always has a small peak below 200 km, and the Ti enhancement always corresponds to large Vo.

3.4 3D ionospheric plasma properties of the space hurricane

Figure 6 shows the 3D plasma parameters of the space hurricane near the three specific altitudes (150 km, 250 km, and 350 km) measured by 11 beams of RISR-N. Linear interpolation was performed on the gate data on each beam. The 11 beams can be divided into three groups corresponding to the azimuth angle: the left three beams (G1), mid five beams (G2), and right three beams (G3). The two-dimensional top view is shown in a small window in the top-right of each panel, which includes the complete measurement results at altitudes of 100–400 km, and only one of the five beams in G2 is shown to prevent overlap. The different azimuth angles and elevation angles enable the beams to measure the plasma properties of different regions near the space hurricane at the same time.

At 18:12 UT, Figures 6A,C show that the beams of G2 and G3 are on the right side of the main auroral structure of the space hurricane and near a possible spiral arm (marked by a red arrow in Figure 6C). In the low-altitude region (within the red dashed box), Ti significantly increased, which corresponds to the large negative

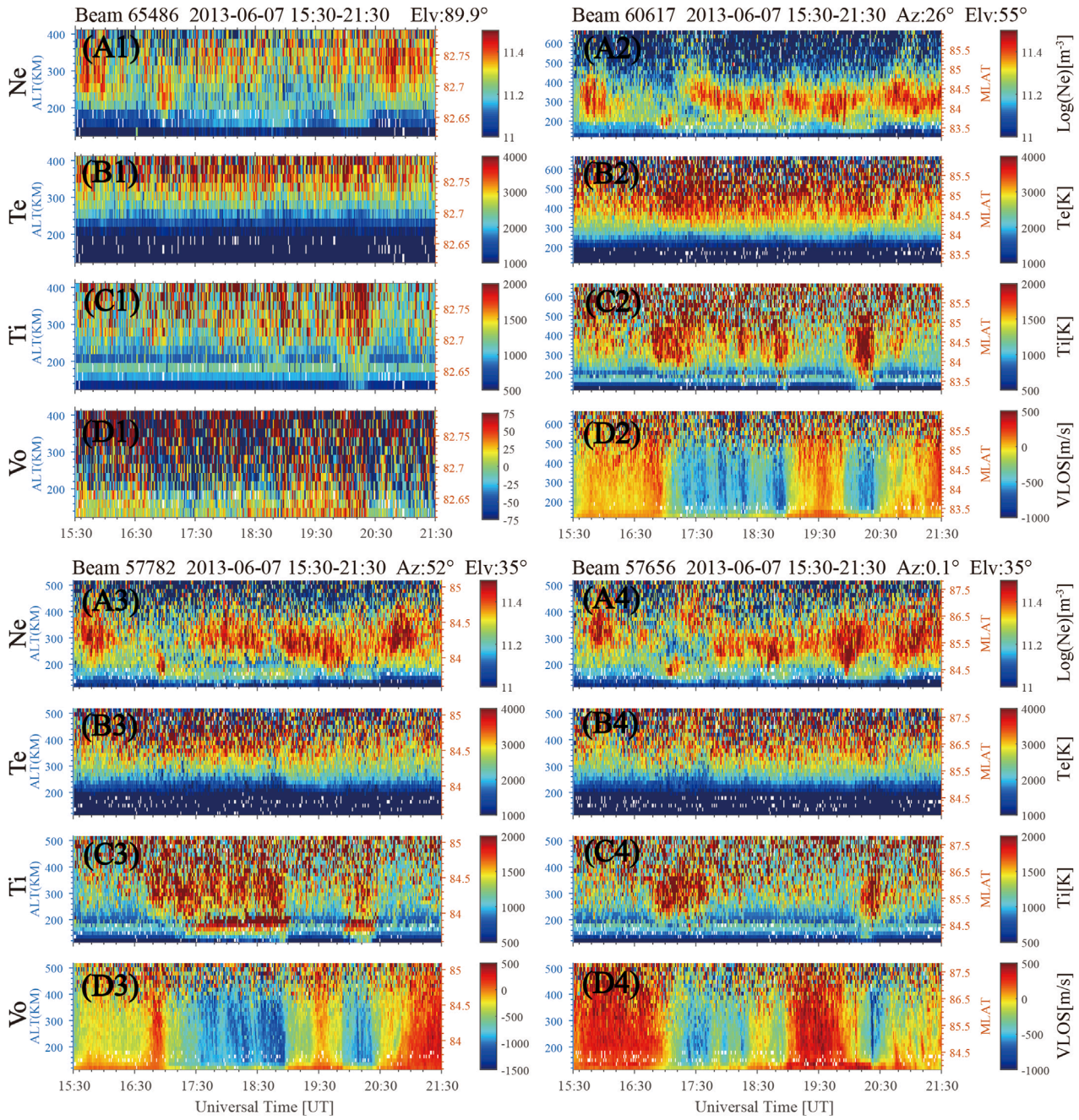

FIGURE 5
Observed plasma parameters from the other four beams of RISR-N during the space hurricane. **(a1–d1)** Observation results of the vertical beam. **(a2–d2)** Results of a beam with the same azimuth angle but a different elevation angle from beam 56954. **(a3–d3)** and panels **(a4–d4)** show the results of two beams with different azimuth angles but the same elevation angle as beam 56954. Panels from top to bottom are electron density (Ne), electron temperature (Te), ion temperature (Ti), and line-of-sight velocity (Vo). The altitude/mapped magnetic latitude are shown to the left/right of each panel. The azimuth angle and elevation angle for each beam are shown in the title.

Vo (>1,000 m/s). This may indicate that Joule heating can be caused by intense electric fields that drive the F-region ion drift at the spiral arm and also the intense currents in the E-region. This result is also consistent with the observation shown in Figure 4E. In addition, due to the beams of G1 being directly above the space hurricane at this time, these beams show lower flow, which cannot effectively cause Joule heating and Ti enhancement.

At 19:51 UT, Figures 6B,D show that G1 is located on the left of the space hurricane, G2 is directly above it, and G3 is located on its right. In Figure 6D, G1 and G3 measured an opposite Vo (red and cyan, respectively), while G2 measured an ~0 velocity (yellow), which can reflect the strong circular horizontal flow around the space hurricane, consistent with the results given in Figure 3. In addition, compared to the larger velocity (~1,000 m/s) measured

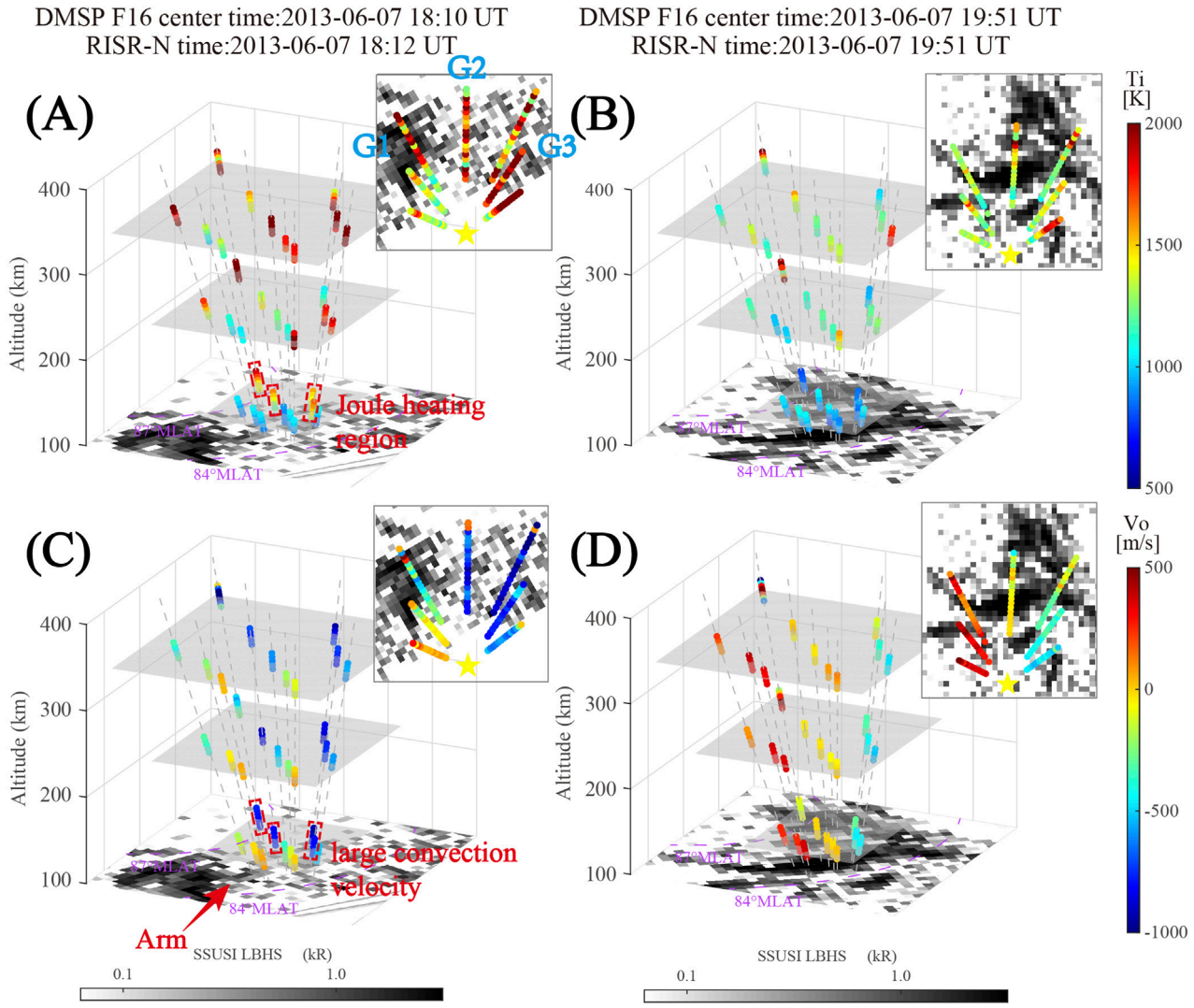

FIGURE 6
3D plasma parameters from 11 beams of RISR-N overlaid on two space hurricane images: **(A, B)** measured Ti at the two space hurricane times; **(C, D)** measured Vo. In each panel, the altitudes of the three gray planes are 150 km, 250 km, and 350 km, respectively. The thin dashed lines represent the complete coverage range of the 11 beams, and only the gates within a 10-km range near each gray plane display their measurement results. The 11 beams can be divided into three groups (G1, G2, and G3) corresponding to the azimuth angle. The two-dimensional top view of each panel is shown in a small window in the top right, which include the complete measurement results at altitudes of 100–400 km, and only one of the five beams in G2 pointing toward magnetic north is shown to prevent overlap. The red thin arrow in **(C)** points out a possible spiral arm of the space hurricane.

by the beams of G2 and G3 at 18:12 UT, the velocity (<500 m/s) measured by G1–G3 at 19:51 UT is much smaller, which may be due to their closer position to the main auroral structure of the space hurricane (also the center of the convective cell). Therefore, no Ti enhancements are shown in Figure 6B due to insufficient heating. After 19:51 UT, the space hurricane moved to the dawn side due to the changing IMF clock angle, so RISR-N can again detect the strong flow shear of the space hurricane shown in Supplementary Movie S1 and Figure 4.

4 Discussion

In this paper, we provide new observed features of the space hurricane in the ionosphere. The results agree well with the high-latitude lobe reconnection mechanism proposed by Q. H. Zhang et al. (2021) with the following implications.

4.1 The space hurricane is embedded in a clockwise lobe convection cell

A statistical study has shown that the space hurricane in the Northern Hemisphere mainly occurs under the conditions of the northward IMF dominated by a positive By component (Lu et al., 2022), which significantly affects the ionospheric convection pattern in the polar cap. Under a northward IMF condition with a small IMF By component, the two lobe cells inside the polar cap showing sunward flow are roughly of the same size (spatially and in voltage)

and symmetrical due to lobe convection (Lockwood and Moen, 1999). However, as |By| increases, one grows and the other shrinks due to the tension force on the newly reconnected field lines. Therefore, for most By values, the polar cap has a three-cell pattern with only one "stirring" circulation flow cell (growing lobe cell) (Huang et al., 2000; Lockwood, 2023). In addition, due to the dipole tilt effect, this circulation seems to occur only in the polar cap of the summer hemisphere, which is more conducive to the lobe reconnection (Crooker and Rich, 1993; Koustov et al., 2017; Lockwood, 2023). For the IMF conditions shown in Figure 1G, the large positive By component makes the clockwise lobe cell fill the whole polar cap and dominate the flow in the Northern Hemisphere. The SuperDARN convection velocity (Figure 3) shows that the space hurricane is surrounded by clockwise convection, which shows that the space hurricane is embedded in a clockwise circulation cell.

4.2 Joule heating effect caused by the space hurricane

To investigate the relationship between Ti enhancements and convection velocity shown in Figures 4, 5, we estimated the Joule heating rate from the convective electric field ($E_{V\times B}$) using the RISR-N observations. As described in *Data and Methodology*, empirical models were used to obtain certain unobserved parameters, such as neutral and ion composition. These empirically derived parameters were used solely to construct a background polar cap condition and do not take into account the effects of neutral components, electron precipitation, and strong convective shear during a space hurricane, so using these parameters result in an error in the peak altitude of the Joule heating rate. For example, the electron precipitation should cause an increase in the local Pedersen conductivity, but the conductivity calculated by empirical models remained unchanged. Therefore, the underestimated Pedersen conductivity at and above the altitude of precipitating electrons leads to the underestimation of the peak altitude of the Joule heating rate.

Although the use of empirical formulas may introduce some bias, the results given in Figure 4E still provide a basis for inferring that 1) the Ti enhancement in the lower altitude is mainly caused by Joule heating due to the large σ_p at low altitude and the large $E_{V\times B}$ from the convection velocity and 2) the Ti enhancement at high altitude is only partly contributed by Joule heating since σ_p sharply decreases with altitude (Brekke et al., 1991; Nishimura et al., 2021) but may be contributed by the upward transport of lower-altitude heating (Huang et al., 2012).

4.3 Characteristics of the spiral arms of the space hurricane

Figure 4 shows that the Ti enhancement corresponds one by one to the sunward Vo from 17:00 to 19:00 UT. Unfortunately, due to the low temporal resolution of DMSP/SSUSI auroral observations, the Ti enhancement structures observed by RISR-N cannot be matched accurately with the aurora structure of the space hurricane. Here, we provide a possible explanation for these structures. We suggest that the multiple flow shears are features when the radar beam sweeps over the spiral arms of the space hurricane. Each spiral arm is surrounded by the large flows to form a local Joule heating region.

We suspect that these structures correspond to the spiral arms because of their regularity. Each Ti enhancement occurs every 10~20 min and lasts approximately 5~15 min, which may correspond to multiple spiral arms or multiple radar sweeps across the same spiral arm. Similar to the model proposed by Southwood (1987), the auroral enhancement of a spiral arm may correspond to an upward FAC region resulting from the flow shear across the arm (L. R. Lyons, 1980; Lyons, L. 1981; Lyons, L. R. 1981). It is the superposition of the clockwise flow near the spiral arm and the local sunward flow caused by the main structure of the space hurricane that lead the radar beam to detect a large sunward flow and Joule heating, as shown in Figures 4A,C. Similar spiral arm structures with flow shears have been found in previous studies. Ma et al. (2021) observed the spiral arms of the westward traveling surge and indicated that there was a strong flow shear around the arm. The auroral spiral is also a prominent vortex structure with spiral structures in optical data (e.g., Davis and Hallinan, 1976; Hu et al., 2013; Lyatsky et al., 2001), and it has been found that the power is provided by two oppositely rotating plasma flow vortices (Keiling et al., 2009).

5 Conclusion

In this paper, we obtained the 3D plasma features of a space hurricane at ionospheric altitudes (100–400 km) for the first time. Based on the plasma velocity observations by three independent instruments, we found that the space hurricane is surrounded with strong circular horizontal plasma flows and embedded in the afternoon lobe convection cell. Based on the plasma measurements from RISR-N, we found that the space hurricane was associated with strong flow shears, downward ionospheric electron transport, and Ti enhancement. Finally, we estimated the Joule heating rate based on the model and observation results and suggest that the multiple Ti enhancements corresponding to the large flow is caused by Joule heating adjacent to the space hurricane's spiral arms, which is an important addition to the total energy deposition in the ionosphere–thermosphere system. These results reveal, for the first time, the characteristics of space hurricanes at low ionospheric altitude, which is of great significance for understanding the magnetospheric ionospheric coupling system under northward IMF conditions.

Data availability statement

The original contributions presented in the study are included in the article/Supplementary Material; further inquiries can be directed to the corresponding author.

Author contributions

SL: writing–original draft and writing–review and editing. Z-YX: supervision, writing–original draft, and writing–review and editing. Q-HZ: supervision and writing–review and editing. YZ:

data curation and writing–review and editing. KO: methodology, visualization, and writing–review and editing. LL: methodology, visualization, and writing–review and editing. ML: formal analysis, methodology, and writing–review and editing. Y-ZM: funding acquisition, project administration, and writing–review and editing. X-YW: data curation, formal analysis, methodology, and writing–review and editing. NB: writing–review and editing. H-GY: funding acquisition, project administration, and writing–review and editing. YW: data curation, investigation, and writing–review and editing. Z-XD: funding acquisition, validation, and writing–review and editing. TX: project administration, resources, and writing–review and editing. S-JS: funding acquisition, resources, and writing–review and editing.

Funding

The author(s) declare that financial support was received for the research, authorship, and/or publication of this article. The work in China was supported by the National Natural Science Foundation of China (Grants 42474219, 42325404, and 42120104003), the International Partnership Program of the Chinese Academy of Sciences (Grant 183311KYSB20200003), the Natural Science Foundation of Shandong Province (Grant ZR2022MD034), the Stable-Support Scientific Project of China Research Institute of Radiowave Propagation (Grant A132312191), the Foundation of the National Key Laboratory of Electromagnetic Environment (Grant JCKY2022210C614240301), the National Program on Key Basic Research Project (2022-173-SD-1), Xiaomi Young Talents Program, the Chinese Meridian Project, and the China Postdoctoral Science Foundation (Grant 2021M701974). The work in Norway was supported by the Research Council of Norway (Grant 223252). The work at UCLA was supported by the NSF grant 20211402.

Acknowledgments

The authors acknowledge the Johns Hopkins University Applied Physics Laboratory for providing the DMSP/SSUSI data (https://ssusi.jhuapl.edu/gal_Aur). The DMSP SSJ/5 and SSM data measured by DMSP F16–F18 were obtained from the National Centers for Environmental Information (NCEI) database. The cross-track velocity data measured by DMSP satellites and RISR-N data were obtained from the Madrigal database (http://cedar.openmadrigal.org/ftp/). The THEMIS Fluxgate Magnetometer (FGM) data are available at http://themis.ssl.berkeley.edu/data/themis/thb/l2/fgm/. The SuperDARN database (http://vt.superdarn.org/plot/map) provided available convection data. The authors thank the working group of IRI, IGRF, and MSIS-E-00 models for providing them freely in MATLAB code from the links https://www.mathworks.com/matlabcentral/fileexchange/34863-international-reference-ionosphere-iri-model, https://www.mathworks.com/matlabcentral/fileexchange/34388-international-geomagnetic-reference-field-igrf-model and https://www.mathworks.com/matlabcentral/fileexchange/40333-msis-e-00.

Conflict of interest

The authors declare that the research was conducted in the absence of any commercial or financial relationships that could be construed as a potential conflict of interest.

The author(s) declared that they were an editorial board member of Frontiers, at the time of submission. This had no impact on the peer review process and the final decision.

Generative AI statement

The author(s) declare that no Generative AI was used in the creation of this manuscript.

Publisher's note

All claims expressed in this article are solely those of the authors and do not necessarily represent those of their affiliated organizations, or those of the publisher, the editors, and the reviewers. Any product that may be evaluated in this article, or claim that may be made by its manufacturer, is not guaranteed or endorsed by the publisher.

Supplementary material

The Supplementary Material for this article can be found online at: https://www.frontiersin.org/articles/10.3389/fspas.2024.1507824/full#supplementary-material

References

Angelopoulos, V. (2008). The THEMIS mission. *Space Sci. Rev.* 141 (1–4), 5–34. doi:10.1007/s11214-008-9336-1

Bahcivan, H., Tsunoda, R., Nicolls, M., and Heinselman, C. (2010). Initial ionospheric observations made by the new Resolute Incoherent Scatter Radar and comparison to solar wind IMF. *Geophys. Res. Lett.* 37, L15103. doi:10.1029/2010GL043632

Berkey, F. T., Cogger, L. L., Ismail, S., and Kamide, Y. (1976). Evidence for a correlation between Sun-aligned arcs and the interplanetary magnetic field direction. *Geophys. Res. Lett.* 3 (3), 145–147. doi:10.1029/GL003i003p00145

Brekke, A., and Hall, C. (1988). Auroral ionospheric quiet summer time conductances. *Ann. Geophysicae-Atmospheres Hydrospheres Space Sci.* 6 (4), 361–375. doi:10.1029/GL015i006p00561

Brekke, A., Moen, J., and Hall, C. (1991). Studies of the conductivities in the auroral-zone ionosphere. *J. Geomagnetism Geoelectr.* 43, 441–465. doi:10.5636/jgg.43.Supplement1_441

Cai, L., Kullen, A., Zhang, Y., Karlsson, T., and Vaivads, A. (2021). DMSP observations of high-latitude dayside aurora (HiLDA). *J. Geophys. Res. Space Phys.* 126 (4). doi:10.1029/2020JA028808

Crooker, N., and Rich, F. (1993). Lobe cell convection as a summer phenomenon. *J. Geophys. Research-Space Phys.* 98 (A8), 13403–13407. doi:10.1029/93JA01037

Davis, T., and Hallinan, T. (1976). Auroral spirals .1. Observations. *J. Geophys. Research-Space Phys.* 81 (22), 3953–3958. doi:10.1029/JA081i022p03953

Fear, R. C., and Milan, S. E. (2012). The IMF dependence of the local time of transpolar arcs: implications for formation mechanism. *J. Geophys. Res. Space Phys.* 117 (A3), n/a-n/a. doi:10.1029/2011JA017209

Frey, H. U., Han, D., Kataoka, R., Lessard, M. R., Milan, S. E., Nishimura, Y., et al. (2019). Dayside aurora. *Space Sci. Rev.* 215 (8), 51. doi:10.1007/s11214-019-0617-7

Frey, H. U., Immel, T. J., Lu, G., Bonnell, J., Fuselier, S. A., Mende, S. B., et al. (2003). Properties of localized, high latitude, dayside aurora. *J. Geophys. Res.* 108 (A4), 8008. doi:10.1029/2002JA009332

Fujii, R., Nozawa, S., Buchert, S. C., and Brekke, A. (1999). Statistical characteristics of electromagnetic energy transfer between the magnetosphere, the ionosphere, and the thermosphere. *J. Geophys. Research-Space Phys.* 104 (A2), 2357–2365. doi:10.1029/98JA02750

Greenwald, R. A., Baker, K. B., Hutchins, R. A., and Hanuise, C. (1985). An HF phased-array radar for studying small-scale structure in the high-latitude ionosphere. *Radio Sci.* 20 (1), 63–79. doi:10.1029/rs020i001p00063

Han, D.-S., Feng, H.-T., Zhang, H., Zhou, S., and Zhang, Y. (2020). A new type of polar cap arc observed in the ~1500 MLT sector: 1. Northern hemisphere observations. *Geophys. Res. Lett.* 47 (20), e2020GL090261. doi:10.1029/2020GL090261

Hardy, D. A., Schmitt, L. K., Gussenhoven, M. S., Marshall, F. J., and Yeh, H. C. (1984). Precipitating electron and ion detectors (SSJ/4) for the block 5D/flights 6-10 DMSP (Defense Meteorological Satellite Program) satellites: calibration and data presentation. *Rep. AFGL-TR-84-0317. Air Force Geophys.*

Heinselman, C. J., and Nicolls, M. J. (2008). A bayesian approach to electric field and E-region neutral wind estimation with the poker flat advanced modular incoherent scatter radar. *Radio Sci.* 43, RS5013. doi:10.1029/2007RS003805

Hosokawa, K., Kullen, A., Milan, S., Reidy, J., Zou, Y., Frey, H. U., et al. (2020). Aurora in the polar cap: a review. *Space Sci. Rev.* 216 (1), 15. doi:10.1007/s11214-020-0637-3

Hu, Z.-J., Yang, H.-G., Hu, H.-Q., Zhang, B.-C., Huang, D.-H., Chen, Z.-T., et al. (2013). The hemispheric conjugate observation of postnoon "bright spots"/auroral spirals. *J. Geophys. Research-Space Phys.* 118 (4), 1428–1434. doi:10.1002/jgra.50243

Huang, C.-S., Sofko, G. J., Koustov, A. V., Andre, D. A., Ruohoniemi, J. M., Greenwald, R. A., et al. (2000). Evolution of ionospheric multicell convection during northward interplanetary magnetic field with $|z/y| > 1$. *J. Geophys. Res. Space Phys.* 105 (A12), 27095–27107. doi:10.1029/2000JA000163

Huang, Y., Richmond, A. D., Deng, Y., and Roble, R. (2012). Height distribution of Joule heating and its influence on the thermosphere. *J. Geophys. Research-Space Phys.* 117, A08334. doi:10.1029/2012JA017885

Keiling, A., Angelopoulos, V., Weygand, J. M., Amm, O., Spanswick, E., Donovan, E., et al. (2009). THEMIS ground-space observations during the development of auroral spirals. *Ann. Geophys.* 27 (11), 4317–4332. doi:10.5194/angeo-27-4317-2009

Korth, H., Anderson, B. J., Frey, H. U., Immel, T. J., and Mende, S. B. (2004). Conditions governing localized high-latitude dayside aurora. *Geophys. Res. Lett.* 31 (4), L04806. doi:10.1029/2003GL018911

Koustov, A. V., Yakymenko, K. N., and Ponomarenko, P. V. (2017). Seasonal effect for polar cap sunward plasma flows at strongly northward IMF *z*. *J. Geophys. Research-Space Phys.* 122 (2), 2530–2541. doi:10.1002/2016JA023556

Kullen, A. (2012). "Transpolar arcs: summary and recent results," in *Geophysical monograph series*. Editors A. Keiling, E. Donovan, F. Bagenal, and T. Karlsson (Washington, D. C.: American Geophysical Union), 69–80. doi:10.1029/2011GM001183

Kullen, A., Fear, R. C., Milan, S. E., Carter, J. A., and Karlsson, T. (2015). The statistical difference between bending arcs and regular polar arcs. *J. Geophys. Res. Space Phys.* 120 (12). doi:10.1002/2015JA021298

Kurihara, J., Oyama, S., Nozawa, S., Tsuda, T. T., Fujii, R., Ogawa, Y., et al. (2009). Temperature enhancements and vertical winds in the lower thermosphere associated with auroral heating during the DELTA campaign: DELTA CAMPAIGN. *J. Geophys. Res. Space Phys.* 114 (A12), n/a. doi:10.1029/2009JA014392

Lamarche, L. J., Varney, R. H., and Reimer, A. S. (2021). Ion heating in the polar cap under northwards IMF Bz. *J. Geophys. Res. Space Phys.* 126, e2021JA029155. doi:10.1029/2021JA029155

Liou, K., Newell, P. T., Meng, C.-I., Brittnacher, M., and Parks, G. (1998). Characteristics of the solar wind controlled auroral emissions. *J. Geophys. Res. Space Phys.* 103 (A8), 17543–17557. doi:10.1029/98JA01388

Lockwood, M. (2022). Solar wind—magnetosphere coupling functions: pitfalls, limitations, and applications. *Space weather.* 20 (2). doi:10.1029/2021SW002989

Lockwood, M. (2023). Northern and Southern Hemisphere Polar Cap Indices: to what extent do they agree and to what extent should they agree? (preprint). *Preprints*. doi:10.22541/essoar.167839723.36592704/v1

Lockwood, M., and Moen, J. (1999). Reconfiguration and closure of lobe flux by reconnection during northward IMF: possible evidence for signatures in cusp/cleft auroral emissions. *Ann. Geophys.* 17 (8), 996–1011. doi:10.1007/s00585-999-0996-2

Lockwood, M., Sandholt, P. E., Cowley, S. W. H., and Oguti, T. (1989). Interplanetary magnetic field control of dayside auroral activity and the transfer of momentum across the dayside magnetopause. *Planet. Space Sci.* 37 (11), 1347–1365. doi:10.1016/0032-0633(89)90106-2

Lu, S., Xing, Z.-Y., Zhang, Q.-H., Zhang, Y.-L., Ma, Y.-Z., Wang, X.-Y., et al. (2022). A statistical study of space hurricanes in the Northern Hemisphere. *Front. Astronomy Space Sci.* 9, 1047982. doi:10.3389/fspas.2022.1047982

Lyatsky, W., Cogger, L. L., Jackel, B., Hamza, A. M., Hughes, W. J., Murr, D., et al. (2001). Substorm development as observed by Interball UV imager and 2-D magnetic array. *J. Atmos. Solar-Terrestrial Phys.* 63 (15), 1609–1621. doi:10.1016/S1364-6826(01)00045-1

Lyons, L. (1980). Generation of large-scale regions of auroral currents, electric potentials, and precipitation by the divergence of the convection electric-field. *J. Geophys. Research-Space Phys.* 85 (NA1), 17–24. doi:10.1029/JA085iA01p00017

Lyons, L. (1981a). Discrete aurora as the direct result of an inferred high-altitude generating potential distribution. *J. Geophys. Research-Space Phys.* 86 (NA1), 1–8. doi:10.1029/JA086iA01p00001

Lyons, L. R. (1981b). The field-aligned current versus electric potential relation and auroral Electrodynamics. *Present. A. T. Phys. Auror. Arc Form. Geophys. Monogr.* 25, 252–259. doi:10.1029/gm025p0252

Ma, Y., Zhang, Q., Lyons, L. R., Liu, J., Xing, Z., Reimer, A., et al. (2021). Is westward travelling surge driven by the polar cap flow channels? *J. Geophys. Res. Space Phys.* 126 (8). doi:10.1029/2020JA028498

Nishimura, Y., Sadler, F. B., Varney, R. H., Gilles, R., Zhang, S. R., Coster, A. J., et al. (2021). Cusp dynamics and polar cap patch formation associated with a small IMF southward turning. *J. Geophys. Research-Space Phys.* 126 (5), e2020JA029090. doi:10.1029/2020ja029090

Nishitani, N., Ruohoniemi, J. M., Lester, M., Baker, J. B. H., Koustov, A. V., Shepherd, S. G., et al. (2019). Review of the accomplishments of mid-latitude super dual auroral radar network (SuperDARN) HF radars. *Prog. Earth Planet. Sci.* 6 (1), 27. doi:10.1186/s40645-019-0270-5

Oksavik, K., van der Meeren, C., Lorentzen, D. A., Baddeley, L. J., and Moen, J. (2015). Scintillation and loss of signal lock from poleward moving auroral forms in the cusp ionosphere. *J. Geophys. Research-Space Phys.* 120 (10), 9161–9175. doi:10.1002/2015JA021528

Prikryl, P., Jayachandran, P. T., Mushini, S. C., Pokhotelov, D., MacDougall, J. W., Donovan, E., et al. (2010). GPS TEC, scintillation and cycle slips observed at high latitudes during solar minimum. *Ann. Geophys.* 28 (6), 1307–1316. doi:10.5194/angeo-28-1307-2010

Prikryl, P., Jayachandran, P. T., Mushini, S. C., and Richardson, I. G. (2014). High-latitude GPS phase scintillation and cycle slips during high-speed solar wind streams and interplanetary coronal mass ejections: a superposed epoch analysis. *Earth Planets Space* 66, 62. doi:10.1186/1880-5981-66-62

Reistad, J. P., Laundal, K. M., Ostgaard, N., Ohma, A., Burrell, A. G., Hatch, S. M., et al. (2021). Quantifying the lobe reconnection rate during dominant IMF b_y periods and different dipole tilt orientations. *J. Geophys. Research-Space Phys.* 126 (11), e2021JA029742. doi:10.1029/2021JA029742

Reistad, J. P., Laundal, K. M., Ostgaard, N., Ohma, A., Haaland, S., Oksavik, K., et al. (2019). Separation and quantification of ionospheric convection sources: 1. A new technique. *J. Geophys. Research-Space Phys.* 124 (7), 6343–6357. doi:10.1029/2019JA026634

Rich, F., and Hairston, M. (1994). Large-scale convection patterns observed by dmsp. *J. Geophys. Research-Space Phys.* 99 (A3), 3827–3844. doi:10.1029/93JA03296

Ruohoniemi, J. M., and Baker, K. B. (1998). Large-scale imaging of high-latitude convection with super dual auroral radar network HF radar observations. *J. Geophys. Res.* 103 (20), 20797–20811. doi:10.1029/98ja01288

Southwood, D. J. (1987). The ionospheric signature of flux transfer events. *J. Geophys. Res.* 92 (A4), 3207–3213. doi:10.1029/JA092iA04p03207

Villain, J.-P., Hanuise, C., and Caudal, G. (1985). A SAFARI-EISCAT comparison between the velocity of F region small-scale irregularities and the ion drift. *J. Geophys. Res.* 90 (A9), 8433–8443. doi:10.1029/ja090ia09p08433

Wang, Y., Cao, Z., Xing, Z.-Y., Zhang, Q.-H., Jayachandran, P. T., Oksavik, K., et al. (2021). GPS scintillations and TEC variations in association with a polar cap arc. *J. Geophys. Research-Space Phys.* 126 (3), e2020JA028968. doi:10.1029/2020JA028968

Xing, Z., Zhang, Q., Han, D., Zhang, Y., Sato, N., Zhang, S., et al. (2018). Conjugate observations of the evolution of polar cap arcs in both hemispheres. *J. Geophys. Res. Space Phys.* 123, 1794–1805. doi:10.1002/2017JA024272

Zhang, Q.-H., Ma, Y.-Z., Jayachandran, P. T., Moen, J., Lockwood, M., Zhang, Y.-L., et al. (2017). Polar cap hot patches: enhanced density structures different from the classical patches in the ionosphere. *Geophys. Res. Lett.* 44 (16), 8159–8167. doi:10.1002/2017GL073439

Zhang, Q.-H., Zhang, Y.-L., Wang, C., Lockwood, M., Yang, H.-G., Tang, B.-B., et al. (2020). Multiple transpolar auroral arcs reveal insight about coupling processes in the Earth's magnetotail. *Proc. Natl. Acad. Sci.* 117 (28), 16193–16198. doi:10.1073/pnas.2000614117

Zhang, Q.-H., Zhang, Y.-L., Wang, C., Oksavik, K., Lyons, L. R., Lockwood, M., et al. (2021). A space hurricane over the Earth's polar ionosphere. *Nat. Commun.* 12 (1), 1207. doi:10.1038/s41467-021-21459-y

Zhang, Y., Paxton, L. J., Zhang, Q., and Xing, Z. (2016). Polar cap arcs: sun-aligned or cusp-aligned? *J. Atmos. Solar-Terrestrial Phys.* 146, 123–128. doi:10.1016/j.jastp.2016.06.001

Zhu, L., Schunk, R. W., and Sojka, J. J. (1997). Polar cap arcs: a review. *J. Atmos. Solar-Terrestrial Phys.* 59 (10), 1087–1126. doi:10.1016/S1364-6826(96)00113-7